International Symposium
On Turbulence and Shear Flow
Phenomena (TSFP-9)
June 30 - July 3, 2015 *Melbourne, Australia*

MANIPULATING FLOW STRUCTURES IN TURBULENT PIPE FLOW

F. Gómez, H. M. Blackburn, M. Rudman
Department of Mechanical
and Aerospace Engineering,
Monash University,
Victoria 3800, Australia
francisco.gomez-carrasco@monash.edu,
hugh.blackburn@monash.edu,
murray.rudman@monash.edu

A. S. Sharma
Faculty of Engineering
and the Environment,
University of Southampton,
Southampton SO17 1BJ, UK
A.Sharma@soton.ac.uk

B. J. McKeon
Graduate Aerospace Laboratories,
California Institute of Technology,
Pasadena, CA 91125, USA
mckeon@caltech.edu

ABSTRACT

Two different tools, the non-empirical resolvent analysis and the data-based dynamic mode decomposition, are employed to assess the changes induced by transpiration in the dynamics of a turbulent pipe flow. The focus is on very large-scale motions. Both analyses permit the observation of streamwise waviness in the large flow structures and how the transpiration can inhibit fluctuation in localized axial positions. We discuss under which conditions an agreement between both methodologies can be achieved.

INTRODUCTION

A deep understanding of the physical mechanisms that act in wall-bounded turbulent flows is required for the design of efficient flow control strategies, as stated by Kim (2011). In this context, recent findings in high-Reynolds number wall-bounded turbulent flows highlight the energetic relevance of coherent structures other than the self-sustaining near-wall cycle (Kim *et al.*, 1987; Jiménez & Pinelli, 1999). These flow structures, known as very large-scale motions (VLSM), were recently reported by Guala *et al.* (2006) and Monty *et al.* (2007) and found to consist of long meandering slender streaks of high and low streamwise velocity that contain a significant fraction of the turbulent kinetic energy and shear stress production. Hence the contribution of these flow structures to the overall wall drag is of utmost importance at very high-Reynolds number. Hutchins & Marusic (2007) observed that these VLSM can reach locations near the wall, thus flow control strategies applied to the wall may have a strong influence on these motions. Consequently, control of these VLSM structures is highly desirable towards a drag increase or reduction in high-Reynolds pipe flow.

Even though computational simulations are almost unaffordable at the Reynolds number in which these structures are energetically dominant, in the sense of producing a second peak in the streamwise turbulent intensity, which occurs for friction Reynolds number $Re_\tau > 10^4$ (Smits *et al.*, 2011), the behavior of these structures can be observed in pipe flow experiments at moderate bulk-flow Reynolds numbers $Re = 12500$, as shown by the proper orthogonal decomposition of experimental data carried out by Hellström *et al.* (2011).

As observed in the seminal work of Choi *et al.* (1994), one of the most potentially effective ways to achieve the manipulation of turbulent flow is the appliance of suction and blowing at the wall, also known as transpiration. The purpose of the present study is to observe how high- and low-amplitude transpiration in pipe flow at a moderate bulk flow Reynolds number $Re = 10000$ can affect the very large-scale motions of the flow. Particularly, we only focus on the effect on the flow of steady wall-normal blowing and suction, that varies sinusoidally in the streamwise direction. To address this, a direct numerical simulation (DNS) dataset for pipe flow at a moderate Reynolds number has been generated. This dataset consists of a wall transpiration parameter sweep in order to assess the effect of the transpiration parameters on the turbulent statistics and identify interesting drag increasing and reducing configurations.

Here we employ the resolvent analysis to identify the flow structures that are amplified/damped by the effect of different transpiration configurations. The resolvent framework (McKeon & Sharma, 2010) consists of an amplification analysis of the Navier–Stokes equations in the wavenumber/frequency domain, which yields a linear relationship between the velocity fields and the non-linear terms sustaining the turbulence, and hence the mean profile though the Reynolds shear stress, via a resolvent operator. This framework has been already successfully employed by Sharma & McKeon (2013) to recreate complex coherent structures, VLSM among them, from a low-dimensional subset of modes. To complement this tool, a dynamic mode decomposition (Schmid, 2010; Rowley *et al.*, 2009) (DMD) analysis on the turbulent DNS data is carried out to provide the most energetic flow structures. Gómez *et al.* (2014)

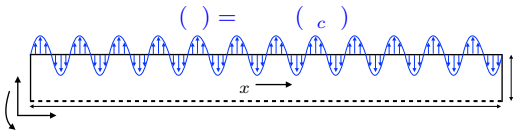

Figure 1. Physical domain and transpiration boundary condition

provided a link between amplification and energy through the similar characteristics exhibited by the most energetically relevant flow structures, arising from a dynamic mode decomposition of direct numerical simulation data of uncontrolled pipe flow, and the resolvent modes associated with the most amplified sparse frequencies. In this paper, we discuss under which conditions such agreement can be achieved.

NUMERICAL METHODOLOGY

A spectral element-Fourier direct numerical simulation (DNS) solver is employed to solve the incompressible Navier–Stokes equations in dimensional form,

$$\nabla \cdot \hat{\mathbf{u}} = 0 \tag{1}$$

$$\frac{\partial \hat{\mathbf{u}}}{\partial t} + \hat{\mathbf{u}} \cdot \nabla \hat{\mathbf{u}} = -\nabla p + \nu \nabla^2 \hat{\mathbf{u}} + \mathbf{f} \tag{2}$$

where ν is the constant kinematic viscosity, $\hat{\mathbf{u}} = (u, v, w)$ is the velocity vector expressed in cylindrical coordinates (x, r, θ), p is the pressure, the density has been fixed to $\rho = 1$ and $\mathbf{f} = (f_x, 0, 0)$ is a forcing vector. A sketch of the configuration in shown in Figure 1, which includes the steady sinusoidal wall-normal flow transpiration along the streamwise direction with an amplitude A and a streamwise wavenumber k_c. Note that k_c must be an integer multiple of the fundamental wavenumber in the axial direction $2\pi/L$ to enforce a a zero net mass flux over the pipe wall. A constant streamwise body force f_x is added in (2) to ensure that the velocity and pressure are streamwise periodic; this force acts as a constant streamwise pressure gradient and hence drives the flow through the pipe. We keep constant the body force constant for all cases. As consequence of momentum balance, the mean wall shear stress τ_w is also kept constant. Hence the friction velocity u_τ and the friction Reynolds number Re_τ are the same for all cases considered.

The numerical method is fully described in Blackburn & Sherwin (2004). A similar mesh as in previous works by Saha *et al.* (2015) at this same $Re_\tau = 314$ is employed. The grid consists of 240 elements in the meridional semi-plane with a 11th-order nodal shape functions and 320 Fourier planes along the azimuthal spatial direction, corresponding to a total of approximately 1.1×10^7 computational nodes. For transpiration cases in which the flow rate is significantly increased, a finer mesh consisting of 1.6×10^7 degrees of freedom has been additionally employed. Simulations are restarted from a snapshot of the uncontrolled pipe flow, transient effects are discarded by inspecting the temporal evolution of the energy of the azimuthal Fourier modes. Typically, 50-100 wash-out times (L/U_b) are required for convergence of the statistics.

SELECTION OF PARAMETERS

The present study deals with a broad parameter space. Namely, the transpiration amplitude A and wavenumber k_c, and the spatial wavenumbers/frequency combination (k, n, ω) of the flow structures subject to study.

Transpiration parameters

The transpiration amplitude A and wavenumber k_c are selected in terms of drag reducing or increasing configurations. Following the classical Reynolds decomposition, the total velocity is decomposed as the sum of the mean flow $\mathbf{u_0}$ and a fluctuating velocity $\mathbf{u}$, which reads

$$\hat{\mathbf{u}}(x, r, \theta, t) = \mathbf{u_0}(x, r) + \mathbf{u}(x, r, \theta, t)\,, \tag{3}$$

with the mean flow obtained by averaging the total flow in time and the azimuthal direction as

$$\mathbf{u_0}(x, r) = \lim_{T \to \infty} \frac{1}{T} \int_0^T \frac{1}{2\pi} \int_0^{2\pi} \hat{\mathbf{u}}(x, r, \theta, t) \mathrm{d}t \mathrm{d}\theta\,. \tag{4}$$

Note that the streamwise spatial dependence of the mean flow permits a non-zero mean in the wall normal direction, hence $\mathbf{u_0}(x, r) = (u_0, v_0, 0)$. Turbulence statistics additionally averaged in the streamwise direction are denoted with a bar

$$\bar{\mathbf{u}}_0(r) = \frac{1}{L} \int_0^L \mathbf{u}_0(x, r) \mathrm{d}x\,. \tag{5}$$

In terms of flow control efficiency, here we defined drag-reducing or -increasing configurations as those that reduce or increase the streamwise flow rate with respect to the smooth pipe. Mathematically,

$$\Delta Q = \frac{\int_0^R \Delta \bar{u}_0 r \mathrm{d}r}{\int_0^R \bar{u}_0^s r \mathrm{d}r} \begin{cases} < 0 \text{ drag-increasing}\,, \\ > 0 \text{ drag-reducing}\,, \end{cases} \tag{6}$$

where $\Delta u_0 = (\bar{u}_0^c - \bar{u}_0^s)$, being c and s superscripts to denote controlled and smooth pipe respectively. Table 1 lists the four cases selected for this study in terms of change in drag. Figure 2 complements Table 1 by showing instant streamwise velocity planar contours for the four cases considered. These contours permit to infer how the flow structures are modified by the transpiration in each of the cases. Note that we consider most appropriate to represent axial velocity because of the streamwise character of the VLSMs.

Flow structures parameters

As discussed in detail by Sharma & McKeon (2013), VLSMs can be represented with resolvent modes of lengths scales $(k, n) = (1, 6)$ and with a convective velocity $c = 2/3$ of the centerline streamwise velocity. This representation is based on the work of Monty *et al.* (2007) and Bailey & Smits (2010), which experimentally investigated the spanwise length scale associated with the VLSM and found to be of the order of the outer length scale, $n = 6$. Here we focus on the wavenumber combination $(k, n, c) = (1, 6, 2/3)$. Note that the convective velocity is non-dimensionalized with the centerline velocity and calculated assuming $k = 1$. Also, this wavenumber corresponds to the largest structure that fits in the computational domain.

Table 1. Transpiration cases considered in this paper

	Case	A	k_c	ΔQ	Re	Re_τ
	reference	-	-	-	10000	314
I	large drag-reduction	0.314	10	0.19	11900	314
II	small drag-reduction	0.022	10	0.04	10400	314
III	drag-increase	0.063	2	-0.36	6400	314

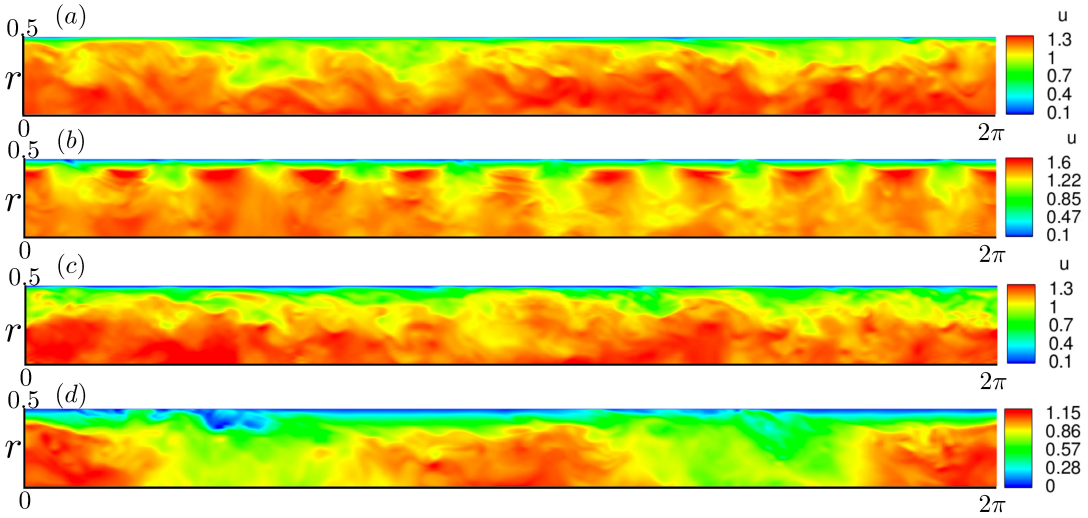

Figure 2. Instant streamwise velocity planar contours for the four cases considered. (a) reference case (b) case I (c) case II (d) case III

APPROACH

The main challenge of incorporating transpiration effects to the resolvent model are the loss of spatial homogeneity in the axial direction and the increase in computational costs associated with their discretization. To address this, the resolvent framework has been extended to two dimensions as previously done by Gómez *et al.* (2014) in order to deal with this spatial non-homogeneity, hence the dependence on the axial coordinate x is retained in the formulation, in contrast with the classical resolvent formulation of McKeon & Sharma (2010). This allows the general analysis of flows non-homogeneous in the axial direction as well as taking into account the finite length of the computational periodic domain employed in the DNS. A Fourier decomposition of the fluctuating velocity leads to

$$\mathbf{u}(x,r,\theta,t) = \sum_n \int_\omega \mathbf{u}_{n,\omega}(x,r) e^{i(n\theta-\omega t)} \mathrm{d}\omega\,, \qquad (7)$$

where n and $\omega/2\pi$ are the non-dimensional azimuthal wavenumber and the temporal frequency respectively. Similarly, the non-linear forcing terms are written as $\mathbf{f}_{n,\omega} = (\mathbf{u}\cdot\nabla\mathbf{u})_{n,\omega}$. Taking this into account, it follows that the Fourier-transformed Navier–Stokes Equation (2) yields the linear relation

$$\mathbf{u}_{n,\omega}(x,r) = \mathscr{H}_{n,\omega}\mathbf{f}_{n,\omega}(x,r)\,, \qquad (8)$$

for each (n,ω) combination. The resolvent operator $\mathscr{H}_{n,\omega}$ acts as a transfer function between the fluctuating velocity and the forcing of the non-linear terms, thus it provides information on which combination of frequencies and wavenumber are damped/excited by wall transpiration effects. A singular value decomposition (SVD) of the resolvent operator

$$\mathscr{H}_{n,\omega} = \sum_m \boldsymbol{\psi}_{n,\omega,m}\sigma_{n,\omega,m}\boldsymbol{\phi}^*_{n,\omega,m} \qquad (9)$$

delivers an input-output amplification relation between singular response modes $\boldsymbol{\psi}_{n,\omega,m}$ and singular forcing modes $\boldsymbol{\phi}_{n,\omega,m}$ through the magnitude of the corresponding singular value $\sigma_{n,\omega,m}$. Each Fourier projection of the non-linear terms can be decomposed as a sum of singular forcing modes to relate the amplification mechanisms to the velocity fields,

$$\mathbf{f}_{n,\omega} = \sum_m \chi_{n,\omega,m}\boldsymbol{\phi}_{n,\omega,m} \qquad (10)$$

where the unknown forcing coefficients $\chi_{n,\omega,n}$ represent the non-linear forcing maintaining the turbulence. A resolvent decomposition of the fluctuating velocity field is then constructed as a weighted sum of singular response modes

$$\mathbf{u}(x,r,\theta,t) = \sum_{\omega,n} \chi_{n,\omega,1}\sigma_{n,\omega,1}\boldsymbol{\psi}_{n,\omega,1} e^{i(n\theta-\omega t)}\Delta\omega\,, \qquad (11)$$

in which the low-rank nature of the resolvent, $\sigma_{n,\omega,1} \gg \sigma_{n,\omega,2}$, can be exploited to create a rank-1 model (Moarref *et al.*, 2013). We note here that, although the rank-1 model has proven to be effective for canonical flows, this simplification may not be adequate for pipe flow with transpiration. Additionally, we remind that this modified resolvent model provides two-dimensional modes $\boldsymbol{\psi}_{n,\omega,1}(x,r)$ containing a range of axial wavenumbers.

To complement the resolvent analysis, a dynamic mode decomposition (Schmid, 2010; Rowley *et al.*, 2009) (DMD) analysis on the turbulent DNS data is carried out to obtain the most energetic flow structures. We employ the DMD algorithm based on the SVD of the snapshot matrix developed by Schmid (2010) with a dataset consisting of 1200 DNS snapshots equispaced during $\mathcal{O}(40)$ wash-out times. As shown by Chen *et al.* (2012), the results from a DMD analysis of a statistically steady flow such as these can be interpreted as a time Fourier analysis. This has been confirmed through obtained values of decay/growth of the DMD eigenvalues close to zero. Hence, the obtained DMD modes are marginally stable, and can be considered Fourier modes. In the next section, we employ the resolvent analysis and DMD to address how the most amplified and energetic flow structures are manipulated by effect of the transpiration. This is the first step to establish a relation between the changes in flow structures and the drag reduction or increase mechanisms.

RESULTS AND DISCUSSION

Figure 3 presents the most amplified and the most energetic flow structures for the four cases listed in Table 1.Figure 3(a) shows a comparison between the amplification obtained from the resolvent analysis and the norm of the most energetic DMD vectors and their associated frequency for the reference case. As explained by Gómez *et al.* (2014), a sparsity is observed in both energy and amplification consequence of a critical layer mechanism and a finite length periodic domain. The diagonal terms of the inverse of the resolvent matrix in (8) for the reference pipe flow, using Cartesian coordinates for easiness in the explanation, read

$$h_{ii}^{-1} = u_0\partial_x u - \partial_t u + Re^{-1}\nabla^2 u, \qquad (12)$$

and considering Fourier modes in the axial direction and time, it follows that

$$h_{ii}^{-1} = \mathrm{i}(u_0 k - \omega)u + Re^{-1}\nabla^2 u, \qquad (13)$$

thus, irrespective of the size of the Laplacian, there is a large amplification if the wavespeed $c = \omega/k$ matches the mean streamwise velocity, i.e, $c = u_0$. That means that flow structures that travel at the local mean velocity create high amplification and hence are greatly amplified. Furthermore, only structures with an integer axial wavenumber, $k_i = 1, 2, \ldots$ can exist in the flow because of the finite length periodic domain. This fact creates energy and amplification sparsity in frequency. Per each integer axial wavenumber k_i there is a frequency ω_i for which the critical layer mechanism occurs, i.e., $\omega_i = k_i c = k_i u_0$. This amplification and energy sparsity behavior is clearly observed in the reference case, as shown in Figure 3(a), in which the peak frequencies are harmonics. We also observe that the frequencies corresponding to the peaks of amplification and energy significantly differ. This fact has been observed by Moarref *et al.* (2013) and Gómez *et al.* (2015) and it is related to the major role that the nonlinear forcing maintaining the turbulence $\chi_{n,\omega,n}$ plays in the decomposition (10). Nevertheless, we observe that the frequency corresponding to the most energetic structures can be found in the proximity of the amplification peaks.

Figure 3(b) and (c) present the principal resolvent mode $\boldsymbol{\psi}_{6,\omega,1}(x,r)e^{\mathrm{i}6\theta}$ and DMD mode corresponding to the most energetic frequency respectively. This frequency is highlighted by an orange arrow. We observe a striking resemblance between the shapes of the principal resolvent mode and the DMD mode and that they match the description of VLSMs. Besides a random shift in phase, both flow structures possess the same dominant axial wavenumber $k = 1$ and same location of maximum/streamwise velocity. Again, we highlight that no streamwise axial wavenumber is imposed, hence the axial wavenumber corresponding to this long structure arise from the singular value decomposition of the resolvent operator.

Figure 3(d)(e)(f) present the results corresponding to the large drag reducing case with transpiration parameters $(A,k) = (0.314, 10)$. We observe that the distribution of amplification is still sparse and high frequencies are amplified with respect to the reference case. The energy represented by the DMD modes is also sparse and indicates that the first frequency peak is still the most energetic one. A disagreement between the principal resolvent mode $\boldsymbol{\psi}_{6,\omega,1}(x,r)e^{\mathrm{i}6\theta}$ and DMD mode corresponding to the most energetic frequency is appreciated. Although both flow structures have the same principal axial wavenumber $k = 1$ modulated by the forcing wavenumber $k_c = 10$, the radial location of the maximum/minimum velocity differs. The location of the maximum/minimum of the resolvent mode is shifted towards the centerline. Also note that the modulation or waviness of the flow structures can be inferred from the corresponding snapshot in Figure 2(b).

We presume that additional sources of high amplification affects the ability of the resolvent operator to represent the flow structures with a rank-1 model. For example, the existence of a non-zero wall-normal velocity at the critical layer adds additional term $v_0\partial_y u$ to (12) and the streamwise gradient of mean axial velocity generates a term $u\partial_x u_0$. The diagonal of the resolvent now reads

$$h_{ii}^{-1} = u_0\partial_x u + v_0\partial_y u + u\partial_x u_0 - \partial_t u + Re^{-1}\nabla^2 u, \qquad (14)$$

hence the location of the maximum/minimum velocity can be shifted. In addition, there are additional sources of high gain, such as streamwise and wall-normal shears in the off-diagonal terms. We recall that resolvent modes represent amplification while DMD modes denote energy, i.e., forcing times amplification. As a consequence, a subset of resolvent modes, properly weighted with their corresponding forcing $\chi_{n,\omega}$, could represent the same structure of the DMD modes.

Results in Figure 3(g)(h)(i) correspond to the small drag reducing case with transpiration parameters $(A,k) = (0.022, 10)$. A significant increase in the amplification of the first peak is the major difference with respect to the reference case in Figure 3(a). Figure 3(h)(i) shows that the shapes of the resolvent and DMD mode agree well. We can observe a slight waviness corresponding to the forcing wavenumber $k_c = 10$ on both modes. We presume that, in

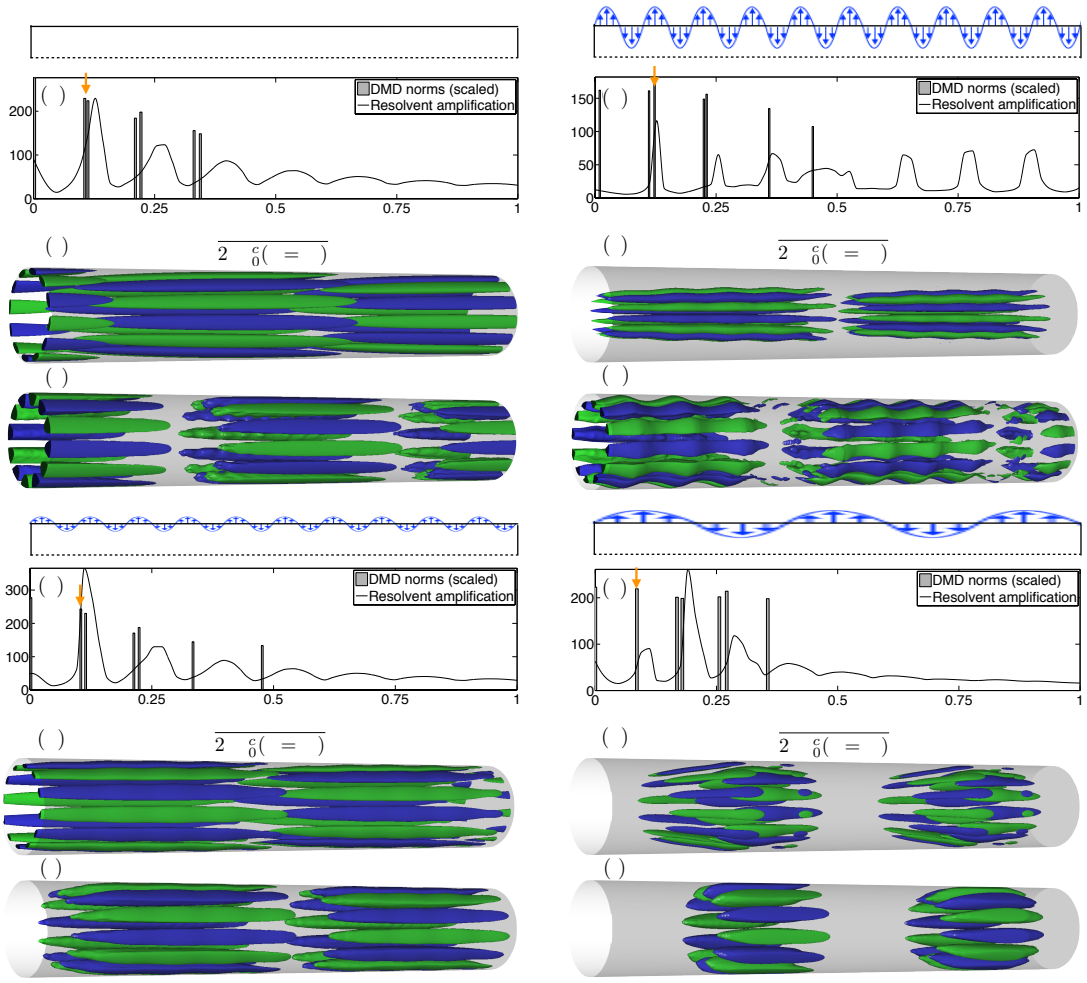

Figure 3. Case III. (a)(d)(g)(j) Comparison between DMD mode norms (bars) from DNS and amplification from resolvent (lines) in frequency at $n = 6$. Iso-surfaces of $1/3$ of the maximum/minimum streamwise velocity of (b)(e)(h)(k) resolvent mode and (c)(f)(i)(l) DMD mode corresponding to frequency highlighted by orange arrow. (a)(b)(c) case reference, (d)(e)(f) case I, (g)(h)(i) case II, (j)(k)(l) case III.

this case, the additional high amplification induced by the transpiration is small since the rank-1 model is able to represent the most energetic flow structure.

The large drag-increase results with transpiration parameters $(A,k) = (0.063,2)$ are presented in Figure 3(j)(k)(l). The peak corresponding to the forcing wavenumber $k = 2$ is highly amplified with respect to the reference case while the rest of peaks are damped. In addition, the DMD norms do not show a decrease with frequency like in the previous cases. They are located around the most amplified frequency. We notice some agreement in the flow structures. Both resolvent and DMD mode show the main axial wavenumber $k = 1$ and two cluster of turbulent activity. These clusters are located in the blowing section of the transpiration. This is consistent with the areas of low and high streamwise velocity observed in the planar snapshot of Figure 2(d). We notice that the resolvent mode has more complexity than the DMD mode, and it contains contribution of the forcing wavenumber $k = 2$. As in the large drag-reducing case, we speculate that the additional high gain induced by the large streamwise gradient of mean velocity limits the ability of the resolvent to reproduce energetic structures with a rank-1 model.

CONCLUSIONS

The changes induced by transpiration in the most energetic flow structures of a pipe flow at the azimuthal wavenumber $n = 6$ have been examined with the resolvent analysis and DMD. In all cases, we have observed that the most relevant flow structures correspond to a streamwise wavenumber $k = 1$. In addition, both analyses have permitted the observation of streamwise waviness in the large flow structures and how the transpiration can inhibit fluctuation in localized axial positions.

For large modifications of the flow, some disagreements have been found between the radial shape of the obtained resolvent and DMD modes. We have hypothesized that a rank-1 resolvent model is insufficient to capture the dynamics of the flow if there are various simultaneous, in a spatial sense, sources of high amplification.

A link between the observed structures and the corresponding mean flow characteristics is a subject of ongoing work.

Acknowledgments

The authors acknowledge financial support from the Australian Research Council through the ARC Discovery Project DP130103103, and from Australia's National Computational Infrastructure via Merit Allocation Scheme Grant D77.

REFERENCES

Bailey, S. C. C. & Smits, A. J. 2010 Experimental investigation of the structure of large-and very-large-scale motions in turbulent pipe flow. *Journal of Fluid Mechanics* **651**, 339–356.

Blackburn, H.M. & Sherwin, S. 2004 Formulation of a Galerkin spectral element–Fourier method for three-dimensional incompressible flows in cylindrical geometries. *J. Comput. Phys.* **197** (2), 759–778.

Chen, K.K., Tu, J.H. & Rowley, C.W. 2012 Variants of dynamic mode decomposition: boundary condition, koopman, and fourier analyses. *Journal of nonlinear science* **22** (6), 887–915.

Choi, H., Moin, P. & Kim, J. 1994 Active turbulence control for drag reduction in wall-bounded flows. *Journal of Fluid Mechanics* **262**, 75–110.

Gómez, F., Blackburn, H. M., Murray, R., McKeon, B. J., Luhar, M., Moarref, R. & Sharma, A. S. 2014 On the origin of frequency sparsity in direct numerical simulations of turbulent pipe flow. *Physics of Fluids* **26** (10), 101703.

Gómez, F., Blackburn, H. M., Murray, R., McKeon, B. J. & Sharma, A. S. 2015 On the coupling of direct numerical simulation and resolvent analysis. In *Progress in Turbulence VI: proceedings of the iTi Conference in Turbulence*. Springer.

Guala, M., Hommema, S.E. & Adrian, R.J. 2006 Large-scale and very-large-scale motions in turbulent pipe flow. *Journal of Fluid Mechanics* **554**, 521–542.

Hellström, L.H.O., Sinha, A. & Smits, A. J. 2011 Visualizing the very-large-scale motions in turbulent pipe flow. *Physics of Fluids (1994-present)* **23** (1), 011703.

Hutchins, N. & Marusic, I. 2007 Evidence of very long meandering features in the logarithmic region of turbulent boundary layers. *Journal of Fluid Mechanics* **579**, 1–28.

Jiménez, J. & Pinelli, A. 1999 The autonomous cycle of near-wall turbulence. *Journal of Fluid Mechanics* **389**, 335–359.

Kim, J. 2011 Physics and control of wall turbulence for drag reduction. *Philosophical Transactions of the Royal Society A: Mathematical, Physical and Engineering Sciences* **369** (1940), 1396–1411.

Kim, J., Moin, P. & Moser, R. 1987 Turbulence statistics in fully developed channel flow at low Reynolds number. *Journal of fluid mechanics* **177**, 133–166.

McKeon, B. J. & Sharma, A. S. 2010 A critical layer framework for turbulent pipe flow. *J. Fluid Mech.* **658**, 336–382.

Moarref, R., Sharma, A. S., Tropp, J.A. & McKeon, B. J. 2013 Model-based scaling of the streamwise energy density in high-Reynolds-number turbulent channels. *J. Fluid Mech.* **734**, 275–316.

Monty, J.P., Stewart, J.A., Williams, R.C. & Chong, M.S. 2007 Large-scale features in turbulent pipe and channel flows. *Journal of Fluid Mechanics* **589**, 147–156.

Rowley, C. W., Mezić, I., Bagheri, S., Schlatter, P. & Henningson, D. S. 2009 Spectral analysis of nonlinear flows. *J. Fluid Mech.* **641**, 115–127.

Saha, S., Klewicki, J.C., Ooi, A.S.H & Blackburn, M.H. 2015 Scaling properties of pipe flows with sinusoidal transversely-corrugated walls. *Submitted* .

Schmid, P. J 2010 Dynamic mode decomposition of numerical and experimental data. *J. Fluid Mech.* **656**, 5–28.

Sharma, A. S. & McKeon, B. J. 2013 On coherent structure in wall turbulence. *J. Fluid Mech.* **728**, 196–238.

Smits, A. J., McKeon, B. J. & Marusic, I. 2011 High-Reynolds number wall turbulence. *Annual Review of Fluid Mechanics* **43**, 353–375.